Human Pathology (2021) 109, 69–79

Human PATHOLOGY

www.elsevier.com/locate/humpath

Original contribution

Trophoblast damage with acute and chronic intervillositis: disruption of the placental barrier by severe acute respiratory syndrome coronavirus 2☆

Larisa Debelenko MD, PhD [a,*], Igor Katsyv MD, PhD [a], Alexander M. Chong BS [b], Leonore Peruyero CLT [a], Matthias Szabolcs MD [a], Anne-Catrin Uhlemann MD, PhD [b]

[a] *Department of Pathology and Cell Biology, Columbia University Irving Medical Center, New York, NY, 10032, USA*

[b] *Department of Medicine, Division of Infectious Diseases, Columbia University Irving Medical Center, New York, NY, 10032, USA*

Received 20 October 2020; revised 18 November 2020; accepted 9 December 2020

Available online 13 December 2020

Keywords:
Placenta;
SARS-CoV-2;
Immunohistochemistry;
qRT-PCR;
Vertical transmission

Summary Severe acute respiratory syndrome coronavirus 2 (SARS-CoV-2) was demonstrated in the placenta; however, the data on the prevalence of placental infection and associated histopathology are limited. To identify the frequency and features of SARS-CoV-2 involvement, we performed a clinicopathologic analysis of 75 placental cases from women infected at the time of delivery and 75 uninfected controls. Placental samples were studied with anti−SARS-CoV-2 immunohistochemistry and/or in situ hybridization. Positive results were confirmed by electron microscopy and quantitative reverse-transcription polymerase chain reaction (qRT-PCR). During delivery, only one woman had symptoms of coronavirus disease 2019, six women reported previous symptoms, and 68 women were asymptomatic. All neonates tested negative for SARS-CoV-2 as per nasopharyngeal swab PCR results. Obstetric histories were unremarkable in 29 of 75 SARS-CoV-2−positive and 8 of 75 SARS-CoV-2−negative women. Placental examination was normal in 12 of 75 infected and 3 of 75 uninfected subjects, respectively. In the remaining cases, placental pathology correlated with obstetric comorbidities without significant differences between SARS-CoV-2−positive and SARS-CoV-2−negative women. SARS-CoV-2 was identified in one placenta of an infected, but asymptomatic, parturient. Viral staining was predominantly localized to the syncytiotrophoblast (STB) which demonstrated marked damage accompanied by perivillous fibrin deposition and mixed intervillositis. A significant decrease of viral titers was detected in the attached umbilical cord compared with the villous parenchyma as per qRT-PCR. SARS-CoV-2 is seldom identified in placentas of infected women. Placental involvement by the

☆ Disclosures: None.

* Corresponding author. Department of Pathology and Cell Biology Columbia University Irving Medical Center, 630 W. 168th Street, Room PH15-1574F, New York, NY, 10032, USA

E-mail address: ld2863@cumc.columbia.edu (L. Debelenko).

https://doi.org/10.1016/j.humpath.2020.12.004

virus is characterized by STB damage disrupting the placental barrier and can be seen in asymptomatic mothers without evidence of vertical transmission.

1. Introduction

First reports on placental findings in severe acute respiratory syndrome coronavirus 2 (SARS-CoV-2)—infected women pointed out increased rates of features associated with maternal and fetal vascular malperfusion (FVM) [1—3]. However, several recent studies attested a lack of significant differences in histopathologic characteristics between SARS-CoV-2—positive and SARS-CoV-2—negative women [4—7]. Placental involvement associated with transmission of the virus to neonates has only been reported in a handful of cases [8—12].

Approximately 88% of women who tested positive for SARS-CoV-2 by universal screening at admission for delivery in our institution have been asymptomatic [13], and no cases of congenital infection have been diagnosed thus far. To date, it is unknown whether the virus can affect the placenta and penetrate the placental barrier in the absence of clinical manifestations of maternal infection.

Here, we compared placental histopathology in conjunction with antenatal and intrapartum histories in cohorts of women who tested positive and negative for SARS-CoV-2 at the time of delivery. We did not detect significant differences in pathological features between the groups; however, one of 75 positive cases showed pathology attributable to SARS-CoV-2 in an asymptomatic mother.

2. Materials and methods

The study was approved by the institutional review board. We performed a retrospective review of placental pathology reports and slides from the files of our pathology department. Pertinent clinical information was extracted from medical records. We included 75 women who tested positive for SARS-CoV-2 as per routine polymerase chain reaction (PCR)—based nasopharyngeal swab testing on admission for labor and delivery at our medical center during the regional peak of the coronavirus disease 2019 (COVID-19) pandemic, from March 20 to June 15, 2020. Maternal SARS-CoV-2 PCR tests were performed within 24 h of placental deliveries. All neonates born to mothers positive for SARS-CoV-2 were also tested by SARS-CoV-2 PCR of nasopharyngeal swabs within 12—72 h after delivery. A control group of 75 women who tested negative was matched for gestational age and parity. Subjects with indeterminate SARS-CoV-2 PCR testing results or reversal of positive to negative testing results were excluded.

Pathology diagnoses and representative slides were rereviewed, and the findings were classified using recommendation of the Amsterdam Placental Workshop Consensus [14].

Immunohistochemistry (IHC) was performed on routine sections of the placental disc with monoclonal antibodies against SARS-CoV-2 spike (mouse monoclonal, clone 1A9 [mAb 1A9], dilution 1:1000; GeneTex, Irvine, CA) and nucleocapsid (rabbit monoclonal, clone 0001 [mAb 001], dilution 1:5000; Sino Biological, Wayne, PA) proteins. In situ hybridization (ISH) was performed using the RNAscope-ProbeV-nCoV2019-S (Advanced Cell Diagnostics, Hayward, CA). The assays were validated using pulmonary tissues obtained at autopsies from patients who died of COVID-19; the validation indicated equally high specificity of SARS-CoV-2 ISH and IHC, with the highest sensitivity of antinucleocapsid IHC.

Sixty-four placentas from infected women were studied using at least one modality, including 4 cases studied by ISH, 21 studied by antispike IHC, and 39 studied by antinucleocapsid IHC, and 11 placentas were studied using combinations of the aforementioned techniques, including 1 studied by antinucleocapsid antibody and ISH, 5 studied by antispike antibody and ISH, 3 studied by antispike and antinucleocapsid antibodies, and 1 studied by all 3 techniques.

The assays were carried out using the Bond-III Fully Automated IHC and ISH Stainer (Leica Biosystems, Vista, CA) according to the manufacturer's recommendations.

The light microscopy images were captured using the Olympus BX41 microscope, DP 26 digital camera, and cellSens imaging software (Life Science Solutions).

For the SARS-CoV-2—positive case, electron microscopy (EM) was performed on the formalin-fixed paraffin-embedded (FFPE) tissue of the placental disc punched of paraffin block, deparaffinized, and reprocessed for EM using the standard protocol for medical biopsies and scoped using the JEOL 1011 instrument (JEOL USA, Peabody, MA).

In addition, RNA was extracted from FFPE tissue using the Quick-RNA FFPE Kit (Zymo Research, Irvin, CA). Separate tissue samples of the villous parenchyma, membranes, and umbilical cord were obtained from paraffin blocks using 2-mm sterile disposable biopsy punches (Miltrex, York, PA) to avoid cross contamination.

Quantitative reverse-transcription PCR (qRT-PCR) was carried out using the SARS-CoV-2 RUO kit (Thermo Fisher Scientific, Waltham, MA), which targets the N1 and N2 sequences of the virus as well as RNase P for RNA control (Integrated DNA Technology, Coralville, Iowa), Taqman 4X master mix, and Quant Studio 3 Real-Time PCR system (Thermo Fisher Scientific). Each assay included a standard curve, using the 2019-nCoV_N_Positive Control (Integrated DNA Technology, Coralville, Iowa), to estimate the viral copies in each reaction. Any sample with an exponential fluorescent curve and threshold cycle (C_t) value lower than 40 is considered positive for SARS-CoV-2 by the Centers for Disease Control and Prevention recommendations [15]. Viral titers were calculated as copy numbers divided by sample mass.

Statistical analysis was performed using R version 3.6.3 (R Foundation for Statistical Computing, https://www.r-project.org/foundation/). Significance of differences in counts of clinical or pathological diagnoses was compared using a one-way chi-square goodness-of-fit test, and *P* values were adjusted for multiple comparisons using the Holm method.

3. Results

3.1. Clinical characteristics and the corresponding placental pathologies

Gestational ages ranged from 33 1/7 to 41 (median 38 5/7) in SARS-CoV-2−negative and 31 2/7 to 41 (median 39) in SARS-CoV-2−positive women. Four placentas were from twin pregnancies (two in each group). In the group of 75 women who were negative for SARS-CoV-2 as per routine RT-PCR nasopharyngeal swab testing, antenatal histories and labors were unremarkable in 8 (10.6%) women, compared with 29 (38.7%) women in the group of 75 SARS-CoV-2−positive women ($P = 0.0005$; Table 1). Clinical diagnoses of nonreassuring fetal heart rate (NRFHR), either remote or immediate to deliveries, or category 2 tracing was significantly more prevalent in the group of SARS-CoV-2−negative women (22 of 75 versus 6 of 75, $P = 0.002$), which reflected high volumes of the placentas from high-risk pregnancies in our pathology practice. Similarly, clinical diagnoses of preeclampsia (PEC) and intrauterine growth restriction (IUGR) were more prevalent among SARS-CoV-2−negative women, but the differences were not significant (Table 1). Neonatal congenital anomalies were more frequently seen in noninfected high-risk deliveries, and one case of intrauterine fetal demise due to a cord accident (tight nuchal cord) was diagnosed in the group of uninfected women.

The pathological findings of maternal vascular malperfusion including decidual arteriopathy, distal villous hypoplasia and hypermaturity, and large infarctions were more frequently observed in the group of SARS-CoV-2−negative women (Table 2). Decidual arteriopathy was seen in one of the 75 SARS-CoV-2−positive women in association with PEC with severe features. Three additional cases showed chronic features of maternal vascular malperfusion (distal villous hypoplasia and villous hypermaturity) in infected women, and these findings also correlated with the clinical diagnosis of PEC. Similarly, IUGR and NRFHR correlated with morphologic features of FVM, which were more frequently diagnosed in the group of SARS-CoV-2−negative women (Table 2). Although the frequencies of chronic inflammatory lesions were practically equal between the groups, chronic lymphoplasmacytic deciduitis was more prevalent in the group of SARS-CoV-2−positive women and chronic villitis was more frequent in the group of SARS-CoV-2−negative women; however, none of the differences were statistically significant. Likewise, although intervillous thrombi were more frequently seen among not-infected women and subchorionic thrombi were seen among infected women, the differences were likely random.

In the group of SARS-CoV-2−positive women, only one subject had symptoms of mild infection at the time of delivery; her antenatal history was remarkable for gestational hypertension, and the placental examination was unremarkable, except for rare scattered meconium-laden macrophages in the amniotic plate. In addition, six women were considered postsymptomatic as they were symptom free at the time of delivery, but reported histories of fever and mild respiratory symptoms 2−4 weeks before delivery. The detailed clinicopathologic characteristics of women with symptomatic SARS-CoV-2 infection are presented in Table 3. The remaining 68 women (91%) were asymptomatic. All neonates tested negative for SARS-CoV-2 as per the nasopharyngeal swab test performed within 12−72 h postpartum, and no cases of early onset infection were reported.

SARS-CoV-2 IHC with antispike or antinucleocapsid antibodies and ISH were negative in 74 of 75 placentas of infected and in all stained placentas of uninfected women. The detailed clinicopathologic features of the positive placental case are presented in the following section.

3.2. SARS-CoV-2 placental involvement

3.2.1. Clinical history

A 33-year-old gravida 3 para 2 presented in labor at 37 weeks of gestation. Her prenatal course was significant for a diet-controlled gestational diabetes (glucose challenge test = 178 mg/dL, glucose tolerance test = 185/201/181, HbA1c = 5.5%). At admission, she tested positive for SARS-CoV-2 as per a routine PCR-based swab test but was asymptomatic and did not require supplemental oxygen. The complete blood count was unremarkable, except for thrombocytopenia (platelets = 112 × 10^3/μL, normal range = 167−−374 × 10^3/μL) and decreased monocytes (2%, normal range = 4−8%). Additional workup revealed

Table 1 Spectrum of underlying clinical obstetric and fetal conditions in SARS-CoV-2−positive and negative subjects.

Clinical diagnosis	Times diagnosed		Chi-square, P value	Adjusted, *P* value
	Positive (N = 75)	Negative (N = 75)		
Normal history and labor	29 (38.7%)	8 (10.6%)	0.0005[a]	0.015[a]
Gestational diabetes	5	4	0.045	1
Gestational hypertension	9	8	0.808	1
Preeclampsia	4	12	0.045	1
Obesity	1	2	0.563	1
Asthma	2	4	0.414	1
Gestational cholestasis	4	0	0.045	1
Gestational thrombocytopenia	0	1	0.313	1
Hemoglobinopathy	1	1	1	1
Factor XI deficiency	0	1	0.317	1
HIV positivity	0	1	0.317	1
HSV-2−positive serologies	1	0	0.317	1
Parainfluenza positivity by PCR	1	0	0.317	1
Rhino/enterovirus positivity by PCR	0	1	0.317	1
Chlamydia infection	1	0	0.317	1
Cerclage	2	0	0.157	1
Myomectomy	0	1	0.317	1
Drug abuse	0	2	0.157	1
Chorioamnionitis (clinically)	2	2	1	1
Positive GBS screen	9	8	0.808	1
History of COVID-19 symptoms	7	0	0.008	0.212
Placental abruption	1	2	0.564	1
PPROM	7	8	0.796	1
IUGR	5	12	0.089	1
NRFHR/category 2 tracing	6	22	0.002	0.067
Fetal congenital anomalies	2	6	0.157	1
IUFD	0	1	0.317	1
Nuchal cord	1	2	0.564	1

Abbreviations: HIV, human immunodeficiency virus; HSV-2, herpes simplex virus type 2; PPROM, preterm premature rupture of membranes; IUGR, intrauterine growth restriction; NRFHT, nonreassuring fetal heart rate; IUFD, intrauterine fetal demise; *P*, probability; COVID-19, coronavirus disease 2019.

[a] Significant difference.

mildly elevated levels of inflammatory markers, including C-reactive protein (39.54 mg/L, normal range = 0.00−10.00 mg/L) and erythrocyte sedimentation rate (52 mm/h, normal range = 0−20 mm/h), as well as increased lactate dehydrogenase (251 U/L, normal range = 135−214 U/L) and D-Dimer (1.34 μg/mL, normal range = 0.00−0.80 μg/mL). Interleukin-6 levels were within normal limits.

She did not receive any treatment for her asymptomatic SARS-CoV-2 infection and gave birth to a healthy baby girl by precipitous uncomplicated vaginal delivery. The patient was advised on appropriate infection control precautions while taking care of the baby and breastfeeding.

The baby's birth weight was 2410 g (in 50 percentile), and the Apgar scores were 9 and 9 at 1 and 5 min, respectively. The girl was healthy looking, vigorous, and passed all standard newborn screens (vital signs, bilirubin, congenital heart disease, and hearing). The neonatal SARS-CoV-2 nasal swab test performed on day 2 postpartum was negative. Viral serology tests were not available at the time.

The mother and the child were discharged on hospital day 2 in good health. Maternal and neonatal health evaluations performed by telephone and video assessments on postpartum days three, four, six, and 40 were unremarkable.

3.2.2. Placental pathology

The gross examination showed a soft yellow-white lesion located under the chorionic plate, occupying approximately 5% of the fetal surface. At low magnification, scattered and confluent lesions were seen in each of the four studied sections in a predominantly subchorionic distribution. Individual lesions involved from several to hundreds of villi each and cumulatively affected approximately 15% of the disc. The lesions were characterized by perivillous fibrin deposition and mild to moderate intervillous inflammation (Fig. 1A). The inflammatory infiltrate was patchy and composed of monocytes/macrophages, neutrophils, and rare lymphocytes (Fig. 1B), highlighted by IHC with CD68, CD15 (Fig. 1B, insert), and CD3,

Table 2 Spectrum and frequencies of placental pathology in SARS-CoV-2−positive and SARS-CoV-2−negative subjects.

Placental findings	Times diagnosed		Chi-square, *P* value	Adjusted, *P* value
	Positive (N = 75)	Negative (N = 75)		
Normal	12 (16%)	3 (4%)	0.020	0.403
Signs of AIUI	15	14	0.853	1
Signs of MVM, overall	11	20	0.106	1
Decidual arteriopathy	1	7	0.034	0.644
DVH/AVM	3	6	0.317	1
Infarctions	5	8	0.405	1
Retroplacental hematoma	2	1	0.564	1
Signs of FVM, overall	6	13	0.108	1
Fetal vascular thrombosis	5	10	0.197	1
Villous stromal vascular karyorrhexis	1	2	0.564	1
Segmental avascular villi	4	4	1	1
Chronic inflammatory lesions, overall	10	11	0.827	1
Chronic villitis	3	7	0.206	1
Chronic deciduitis	6	5	0.763	1
Intervillositis	3	2	0.655	1
Other lesions				
Intervillous thrombosis	3	9	0.083	1
Subchorionic thrombosis	6	2	0.152	1
Chorangiosis	5	6	0.763	1
Chorangioma	1	2	0.564	1
Not specific (VA, MEC, PVFD, <20%)	17	18	0.866	1

Abbreviations: AIUI, ascending intrauterine infection (including chorionitis, chorioamnionitis, chorionic and umbilical vasculitis, and funisitis); DVH, distal villous hypoplasia; AVM, accelerated villous maturation; VA, villous agglutination; MEC, meconium macrophages in membranes; PVFD, perivillous fibrin deposition; *P*, probability.

respectively. Both CD4- and CD8-positive T cells were seen, whereas B-cell and plasma cell markers CD20 and CD79A were negative.

At high magnification, the syncytiotrophoblast (STB) showed signs of cellular injury, including *dusky* nuclei with homogenized chromatin, karyorrhexis, pycnosis, loss of nuclear basophilia, and clearing of cytoplasm with eventual formation of *ghost* cells (Fig. 1C, D, E). No nuclear enlargement and intranuclear or cytoplasmic inclusions were seen. Villous stroma showed reactive vascular proliferation and activated fibroblasts (myofibroblasts) (Fig. 1D, E). Intravillous inflammation was not detected, and villous stromal karyorrhexis was only seldom seen. Phosphotungstic acid hematoxylin staining outlined fibrin precipitated to injured apical surfaces of STB (Fig. 1F). Only rare nodular intravillous fibrin (Fig. 1E) and no significant thrombosis of villous capillaries was observed. The umbilical cord, decidua, and membranes were histologically unremarkable.

In summary, the lesions were patchy and focally confluent, and at low magnification, they resembled villous agglutination with perivillous fibrin deposition. A differential diagnosis of acute ischemia/early infarctions was considered, taking into account marked cellular injury of STB. However, mixed intervillous infiltrate was in favor of an inflammatory and possibly infectious etiology.

Table 3 Clinical and placental pathology in 7 women with symptoms of COVID-19.

COVID-19 status	GA (wk)	Clinical history	Placental pathology
Mildly symptomatic	38 4/7	GHTN	Meconium in the amnion
Postsymptomatic	37	GHTN, cone biopsy, cerclage	Chronic deciduitis
Postsymptomatic	39	GDM type 2	Chronic deciduitis, meconium in the amnion
Postsymptomatic	40 5/7	Obesity, cholestasis, Rh-	Chronic deciduitis, chorangiosis
Postsymptomatic	38	Asthma	Subchorionic thrombus, chorangiosis
Postsymptomatic	39 2/9	Parainfluenza coinfection	FVM (focal avascular villi)
Postsymptomatic	40 5/7	Fetal vascular anomaly	No significant pathology

NOTE. Postsymptomatic status was defined as patients who were asymptomatic at the time of delivery, but had a history of COVID-19−related symptoms 4−2 weeks before.

Abbreviations: GA, gestational age; wk, weeks; GHTN, gestational hypertension; GDM, gestational diabetes mellitus; FVM, fetal vascular malperfusion; COVID-19, coronavirus disease 2019.

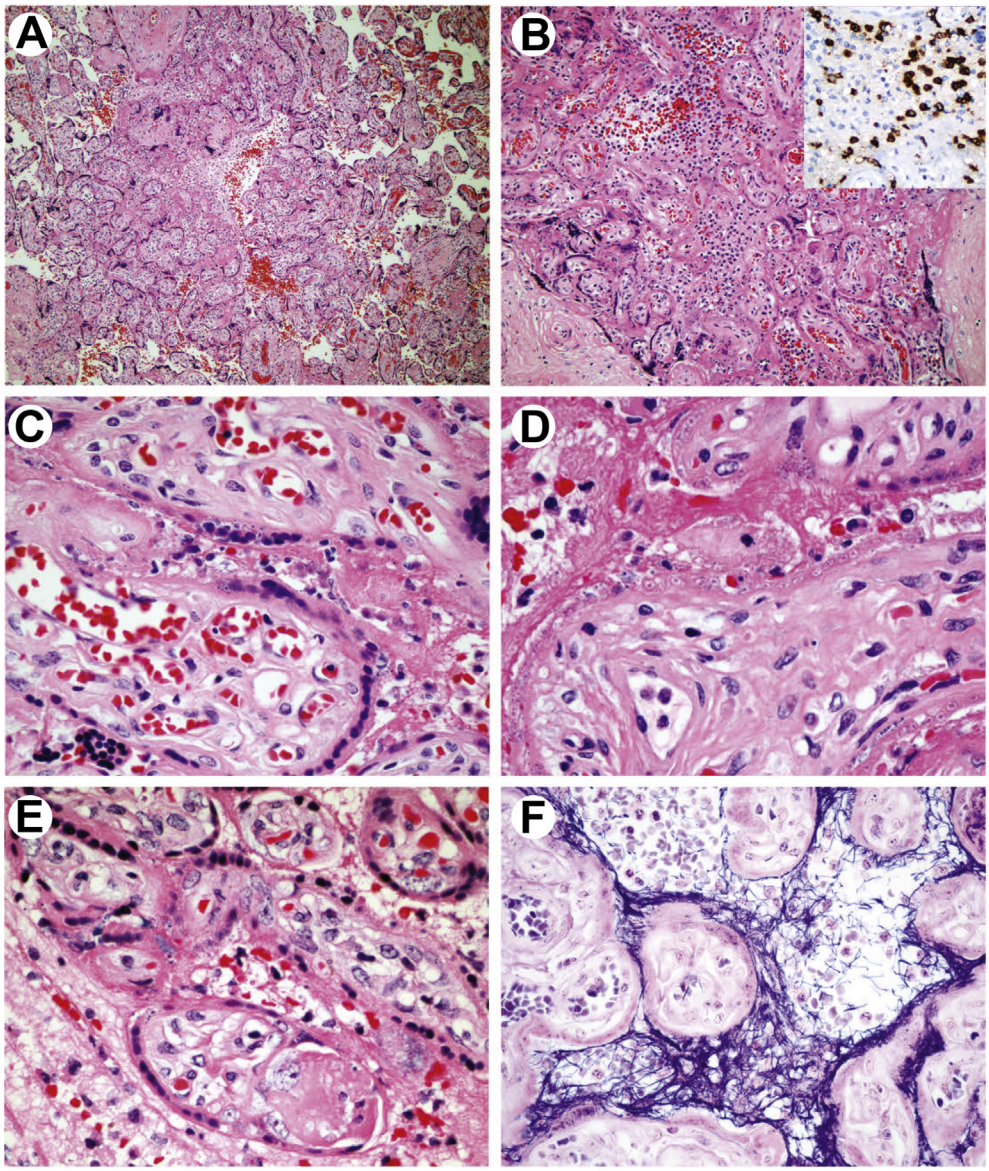

Fig. 1 Placental pathology in SARS-CoV-2 infection. A, Patchy increased villous density, perivillous fibrin deposition and intervillous inflammatory infiltrate (low magnification, H&E). B, Intervillositis with mixed inflammatory infiltrate including a significant population of neutrophils (H&E), stained with CD15 (insert). C, Cellular changes of STB with *dusky* nuclei with homogenized hyperchromatic chromatin and karyorrhexis. Brisk villous capillaries and lack of villous stromal and vascular apoptosis (H&E). D, An advanced stage of STB damage with cytoplasmic clearing and nuclear pycnosis resulting in *ghost* cell appearance (H&E). E, Damaged villi with prominent myofibroblasts. A nodular intravillous fibrin deposition (H&E). F, Perivillous fibrin precipitated to the injured STB highlighted by PTAH special stain. PTAH, phosphotungstic acid hematoxylin; H&E, hematoxylin and eosin; STB, syncytiotrophoblast; SARS-CoV-2, severe acute respiratory syndrome coronavirus 2.

3.2.3. SARS-CoV-2 identification

IHC with antispike mAb 1A9 showed a strong diffuse and granular staining of STB in a patchy distribution (Fig. 2A). ISH with the probe against the spike protein yielded similar, albeit weaker, results (Fig. 2B). In these two assays targeting the spike protein the staining signal was limited to the villous trophoblast and a subset of maternal mononuclear cells in intervillous spaces.

IHC with antinucleocapsid antibody mAb 0001 showed strong patchy staining that included mononuclear blood cells in maternal circulation, STB, and the villous stroma (Fig. 2C). Weak staining of chorionic and amniotic plates,

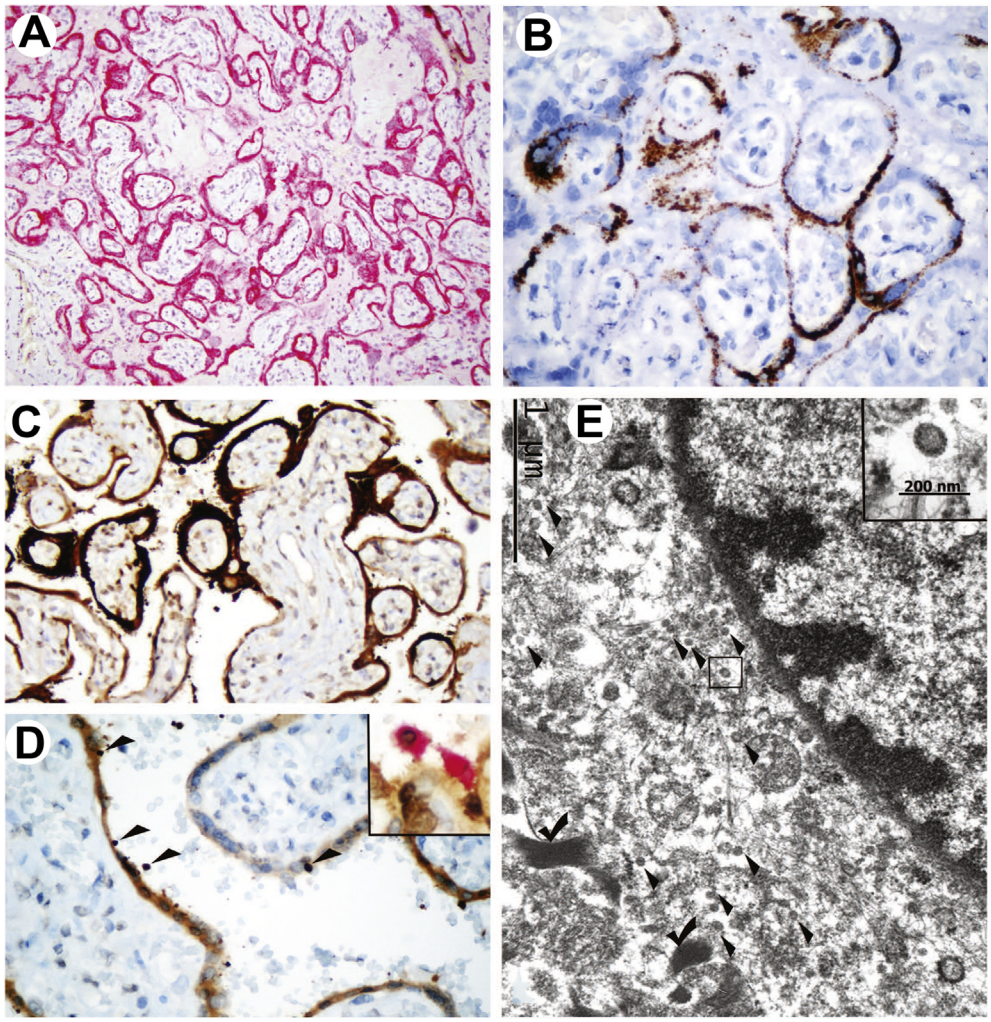

Fig. 2 Identification of SARS-CoV-2 in the placenta. A, Strong diffuse staining of STB with antispike protein antibody (mAb 1A9, red chromogen). B, ISH with spike probe: granular binding pattern in STB. C, IHC with antinucleocapsid mAb 001 strongly positive in STB and a subset of maternal blood cells and weakly positive in the villous stroma. D, IHC with mAb 001: staining of STB and mononuclear cells circulating in maternal vascular spaces (arrowheads). Insert: double staining with mAb (brown chromogen) and CD68 (red chromogen). E, Portion of the villous fibroblast identified by peripheral myofilaments (check marks) with numerous round intracytoplasmic particles, measuring 80−100 nm (arrowheads), consistent with virions. An enlarged virion shown (insert; EM). Bar scales shown. SARS-CoV-2, severe acute respiratory syndrome coronavirus 2; STB, syncytiotrophoblast; IHC, immunohistochemistry; ISH, in situ hybridization. (For interpretation of the references to color in this figure legend, the reader is referred to the Web version of this article.)

including chorionic vessels and the amniotic epithelium, was also observed in the areas that overlay the most prominent subchorionic villous lesions. The decidua, including maternal vessels as well as the attached umbilical cord, was negative for SARS-CoV-2 by IHC and ISH.

Double staining with the mAb 001 (rabbit monoclonal) and CD68 (mouse monoclonal) antibodies demonstrated that maternal blood cells carrying the virus were CD68-positive monocytes/macrophages (Fig. 2D, insert), whereas no double staining was observed with mAb 001 and CD15 or CD3, which label neutrophils and T-lymphocytes, respectively.

EM, performed on the reprocessed FFPE tissue, showed a suboptimally preserved ultrastructure. Numerous round, mildly osmiophilic particles measuring 80−100 nm, consistent with virions, were identified in the cytoplasm of villous fibroblasts (Fig. 2E), while ultrastructural details of trophoblastic cells were lost owing to a combination of cellular necrosis and preservation/reprocessing artifacts.

qRT-PCR was positive for SARS-CoV-2 in the samples of the villous parenchyma, placental membranes, and the umbilical cord, when tested individually punched off paraffin blocks (Fig. 3). The viral titer was, however, significantly higher in the villous parenchyma than in the

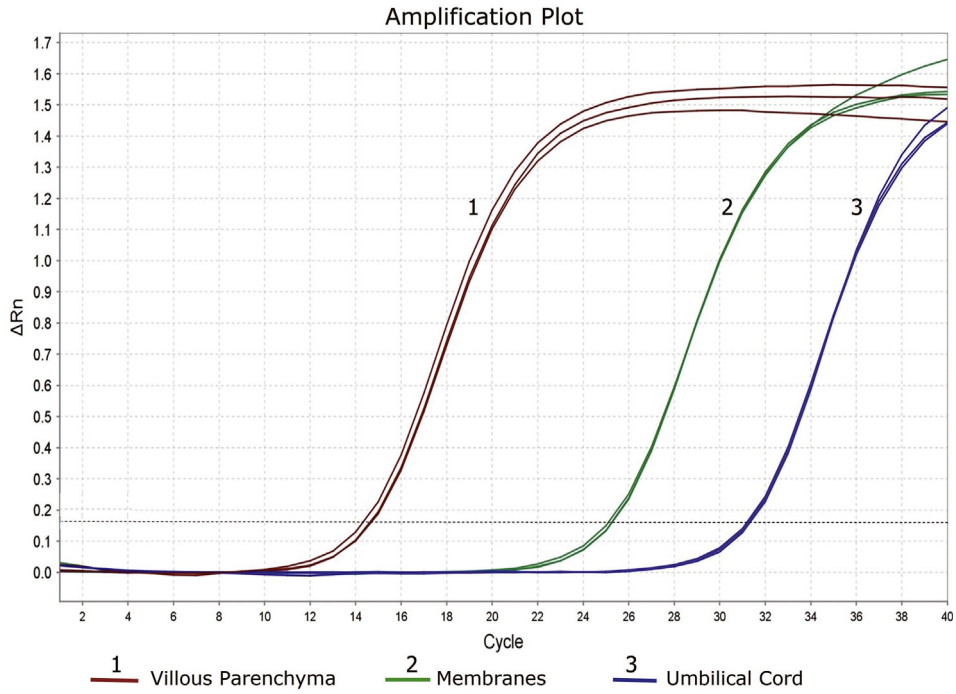

Placental Sample	C_t	Copy Number	RP C_t	Sample Mass (mg)*	Viral Titer (Copies/100 mg)
Villous Parenchyma	14.57	2.08×10^8	22.99	83	2.5×10^8
Membranes	25.22	1.35×10^5	24.12	70	1.92×10^5
Umbilical Cord	31.29	2.05×10^3	22.07	80	2.56×10^3

Fig. 3 SARS-CoV-2 qRT-PCR results in placental samples. Reactions for all samples were run in triplicate with consistent results. C_t (cycle threshold) reflects the number of PCR cycles before the beginning of the exponential phase of the amplification curve. The lower the C_t value, the higher the quantity of the target template in the sample. RP C_t: C_t values of the control RNase P primer/probe set. C_t values of the included viral controls were also obtained (not shown), and along with the standard curve generated in each reaction, they were used for viral copy calculations. *FFPE tissue samples were punched out from the paraffin block and weighted, after removal of excess paraffin and before RNA extraction. SARS-CoV-2, severe acute respiratory syndrome coronavirus 2; qRT-PCR, quantitative reverse-transcription polymerase chain reaction; FFPE, formalin-fixed paraffin-embedded.

membranes and umbilical cord (3 and 5 orders of magnitude, respectively). This correlated with IHC and ISH results showing a strong staining of STB and lack of SARS-CoV-2 reactivity in the cord, with only weak mAb 001 staining of the membranes.

4. Discussion

Until recently, the data on the effects of coronaviruses on pregnancy and placental pathology were scant, with only limited observations published in the aftermath of SARS and Middle East respiratory coronavirus epidemics of 2002−2003 and 2013−2015 [16]. In the current COVID-19 pandemic, several reports described placental pathology in infected women and compared it with different control groups. Our retrospective analysis did not show statistically significant differences in the occurrences of inflammatory or vascular placental pathologies between women infected and not infected at the time of delivery. However, we detected a rare case of SARS-CoV-2 invasion of placental villous tissue associated with intervillositis in an asymptomatic woman.

Previously published studies of the placenta in SARS-CoV-2−positive women were also performed retrospectively and yielded somewhat conflicting results. Shanes et al. [2] observed features of maternal vascular malperfusion, particularly, decidual vasculopathy, in the majority of placentas of women infected with SARS-CoV-2, and this pathology had not been associated with clinical signs of PEC. At the same time, Baergen and Heller [1] reported that although 11 of 20 studied placentas of infected women did not show any significant pathology, the 9 remaining cases exhibited features of FVM (thrombosis and other vaso-occlusive lesions). Increased occurrences of villous agglutination and subchorionic thrombi in 51 positive cases compared with 25 negative controls were detected by Smithgall et al. [3]. At the same time, no characteristic histopathology was found in 19 placentas of infected women, including 2 cases wherein the virus was identified by IHC and ISH by Hecht et al. [5]. Three recent retrospective analyses also did not find detectable histomorphologic features distinguishing placentas of infected and uninfected women, regardless of experienced symptoms of infection [4,6,7], including two cases positive for SARS-CoV-2 by ISH [7].

We observed statistically not significant increases in frequencies of histopathologies associated with maternal and FVM in the group of SARS-CoV-2−negative women in correlation with higher rates of PEC, IUGR, and NRFHT in this group. We explain these findings by sampling bias because only placentas of high-risk cases (approximately 30% of all deliveries in our hospital) are usually submitted for histopathological examination, while a higher percentage (approximately 80%) of SARS-CoV-2−positive cases were considered high risk and sent to pathology regardless of the underlying gestational morbidity during the peak of the COVID-19 pandemic in New York City. Interestingly, the negative correlation between PEC and NRFHT and COVID-19 was also noted by Zhang et al. [7]. This underscores limitations inherent in the methodology of retrospective analysis likely responsible for the conflicting literature results on the overall placental pathology in SARS-CoV-2. A prospective cohort design with the third trimester enrollment and risk stratification might more definitively answer the question whether infection with SARS-CoV-2 increases the incidence of vascular pathology in the placenta.

Our study, however, identified a rare case of placental involvement by SARS-CoV-2, and similar to several other reported cases [8−12], it was associated with intervillositis. In our case, the intervillositis was composed of mixed inflammatory infiltrate, but otherwise, it had features classically described in massive chronic intervillositis (MCI) or chronic histiocytic intervillositis (CHI), namely, marked intervillous inflammation, intervillous fibrin, and trophoblast necrosis [17,18]. Although in most of the cases, this pathology has been associated with alloimmune or autoimmune dysregulations resulting in IUGR and recurrent reproductive loss [19,20], in a small subset of cases, MCI/CHI has infectious etiologies, such as malaria [21] and cytomegalovirus (CMV) infection [22]. While noninfectious MCI/CHI is composed of almost exclusively histiocytes and lymphocytes, intervillositis in infections such as chlamidia, listeriosis, tularemia and others is characterized by a mixed inflammatory infiltrate. The presence of neutrophils may provide a useful diagnostic clue, allowing to suspect infection as a cause of MCI/CHI. Intervillous fibrin and trophoblast necrosis, originally described in MCI/CHI, were prominent in our case of SARS-CoV-2 intervillositis and likely related to the direct injury of STB by SARS-CoV-2. In this respect, the MCI/CHI in SARS-CoV-2 is similar to the diffuse alveolar damage (DAD), in which the virus directly affects the alveolar epithelium, leading to the exposure on the injured cellular surface factors promoting fibrin accumulation. Similar to DAD, the histopathological features of MCI/CHI in SARS-CoV-2 infection are not indicative of the etiology, and only IHC and/or ISH can provide the specific diagnosis.

Direct involvement of STB by SARS-CoV-2 was unexpected because CMV and Zika virus, best known to affect the placenta, are localized to the villous stroma and Hofbauer cells, respectively [22,23], whereas rubella, influenza, and herpes simplex virus (HSV), seldom detected in placental tissue, have been demonstrated in the capillary endothelium and basal plate (rubella) [24], Hofbauer cells and the cytotrophoblast (influenza) [25], and maternal decidualized cells of the decidua capsularis (HSV) [26]. Only in infections caused by coxsackie and Ebola viruses, and Chlamydia, involvement of STB has been shown [27−29]. While data on the levels of constitutive expression of trophoblastic ACE-2 and TMPRSS2 receptors mediating the SARS-CoV-2 cellular entry have been controversial [30,31], our positive case demonstrates that the virus is capable of attaching to and destroying STB.

It has been proposed that detection of the virus in placental villous tissue signifies intrauterine transplacental transmission, which should be distinguished from intrauterine vertical transmission, defined by positive RT-PCR testing of neonates for the virus at or shortly after birth, early onset of symptoms in neonates, and elevated levels of specific IgM antibodies after delivery [32]. Thus, by these criteria, our case exemplifies an intrauterine transplacental transmission in the absence of intrauterine vertical transmission because the neonate was healthy and negative for SARS-CoV-2 by PCR.

Although a vast majority of placentas of infected women have been studied by SARS-CoV-2 IHC and ISH in our institution, only 1 of 126 cases (75 reported here and 51 reported previously [3]) was positive for the virus. Similarly, only rare instances of placental infection were detected by others [5,7]. As per some published and our preliminary data, a higher rate of viral infection is detectable in placental tissue using a more sensitive qRT-PCR analysis, which, however, has limitations because it

cannot differentiate between maternal viremia and viral invasion of the villous tissue.

It would be compelling to hypothesize that transplacental transmission may be associated with hypervirulent SARS-CoV-2 strains; however, Hosier et al. [9] performed the whole-genome sequence comparisons with global isolates and did not find viral mutations in their case of SARS-CoV-2−affected placenta. Some women may also be more susceptible to STB invasion owing to individual genetic polymorphisms regulating cellular entry or cellular defenses. We, however, favor that the viral invasion in the placenta follows the pattern described in the lungs, where the virus was detectable in the alveolar epithelium only during the narrow temporal window of the acute stage of DAD and was cleared off in the organizing DAD [33]. The duration of SARS-CoV-2 infection is 20 days on average, ranging from 5 to 60 days [34]. It may therefore be possible that if the virus reaches and affects the placenta before delivery, it can be cleared and no longer be detectable in a placental specimen obtained at childbirth. Further studies are needed to elucidate the dynamics of SARS-CoV-2 feto-maternal infection.

Unlike in the previously reported SAR-CoV-2−positive placentas [5,7−12], in our case, the SARS-CoV-2 transplacental infection was detected in a patient asymptomatic for COVID-19 and did not result in vertical transmission despite the marked STB damage and high placental viral qRT-PCR titers. It is possible that the premature precipitous delivery prevented further spread of the infection to the infant. However, we also detected significant (in 5 orders of magnitude) decrease of the viral titers in the attached umbilical cord compared with the villous parenchyma; this supports the overall pervasiveness of the placental barrier and suggests that molecular mechanisms shown to govern resistance and antiviral activity of the trophoblast [35] likely play a role in protecting offspring against SARS-CoV-2.

5. Conclusion remarks

Vascular placental pathology seen in placentas of SARS-CoV-2−positive women is largely associated with preexisting maternal and fetal conditions, with no increased rates of decidual arteriopathy or fetal vaso-occlusive lesions in infected women compared with uninfected women. SARS-CoV-2 can be identified in placental tissue in extremely rare cases, wherein the viral particles carried by maternal macrophages attach to and destroy the villous trophoblast, causing acute and chronic intervillositis, similar to some other placental infections. This SARS-CoV-2 placental pathology can be detected in asymptomatic women, while focal penetration of the placental barrier is not always associated with transmission of the infection to offspring.

Acknowledgments

The authors thank Rachel Tucker for the help with specimen sampling and phosphotungstic acid hematoxylin special staining and Zhimin Yu for the help with electron microscopy. L.D. performed conceptualization, data curation, investigation, project administration, supervision, validation, visualization, and writing of the original draft. I.K. performed formal analysis and used software and methodology. A.M.C. performed investigation, used methodology, and carried out validation, visualization, and review and editing. L.P. performed investigation, contributed to methodology. M.S. provided resources and reviewed and edited the manuscript. A.-C.U. performed data curation, investigation, project administration, provided resources, and carried out supervision, validation, visualization, and review and editing.

References

[1] Baergen RN, Heller DS. Placental pathology in covid-19 positive mothers: preliminary findings. Pediatr Dev Pathol 2020;23:177−80. https://doi:10.1177/1093526620925569.

[2] Shanes ED, Mithal LB, Otero S, Azad HA, Miller ES, Goldstein JA. Placental pathology in COVID-19. Am J Clin Pathol 2020;154: 23−32. https://doi:10.1093/ajcp/aqaa089.

[3] Smithgall MC, Liu-Jarin X, Hamele-Bena D, et al. Third trimester placentas of SARS-CoV-2-positive women: histomorphology, including viral immunohistochemistry and in situ hybridization. Histopathology 2020;77:994−9. https://doi: 10.1111/his.14215.

[4] He M, Skaria P, Kreutz K, et al. Histopathology of third trimester placenta from SARS-CoV-2-positive women. medRxiv 2020. https://doi.org/10.1101/2020.08.11.20173005. 08.11.20173005.

[5] Hecht JL, Quade B, Deshpande V, et al. SARS-CoV-2 can infect the placenta and is not associated with specific placental histopathology: a series of 19 placentas from COVID-19-positive mothers. Mod Pathol 2020;2:1−12. https://doi:10.1038/s41379-020-0639-4.

[6] Gulersen M, Prasannan L, Tam HT, et al. Histopathological evaluation of placentas after diagnosis of maternal SARS-CoV-2 infection. Am J Obstet Gynecol MFM 2020 Aug 15:100211. https://doi: 10.1016/j.ajogmf.2020.100211.

[7] Zhang P, Salafia C, Heyman T, Salafia C, Lederman S, Dygulska B. Detection of severe acute respiratory syndrome coronavirus 2 in placentas with pathology and vertical transmission. Am J Obstet Gynecol MFM 2020;3:100197. https://doi:10.1016/j.ajogmf.2020.100197.

[8] Patanè L, Morotti D, Giunta MR, et al. Vertical transmission of COVID-19: SARS-CoV-2 RNA on the fetal side of the placenta in pregnancies with COVID-19 positive mothers and neonates at birth. Am J Obstet Gynecol MFM 2020;2:100145. https://doi:10.1016/j.ajogmf.2020.100145.

[9] Hosier H, Farhadian SF, Morotti RA, et al. SARS-CoV-2 infection of the placenta. J Clin Invest 2020;130:4947−53. https://doi: 10.1172/JCI139569.

[10] Sisman J, Jaleel MA, Moreno W, et al. Intrauterine transmission of SARS-CoV-2 infection in preterm infant. Pediatr Infect Dis J 2020; 39:e265−7. https://doi: 10.1097/INF.0000000000002815.

[11] Vivanti AJ, Vauloup-Fellous C, Prevot S, et al. Transplacental transmission of SARS-CoV-2 infection. Nat Commun 2020;11:3572. https://doi: 10.1038/s41467-020-17436-6.
[12] Hsu AL, Guan M, Johannesen E, et al. Placental SARS-CoV-2 in a pregnant woman with mild COVID-19 disease. J Med Virol 2020. https://doi.org/10.1002/jmv.26386. https://doi: 10.1002/jmv.26386.
[13] Sutton D, Fuchs K, D'Alton M, Goffman D. Universal screening for SARS-CoV-2 in women admitted for delivery. N Engl J Med 2020; 382:2163–4. https://doi: 10.1056/NEJMc2009316.
[14] Khong TY, Mooney EE, Ariel I, et al. Sampling and definitions of placental lesions: Amsterdam placental Workshop group Consensus statement. Arch Pathol Lab Med 2016;140:698–713. https://doi: 10.5858/arpa.2015-0225-CC.
[15] Lu X, Wang L, Sakthivel SK, et al. US CDC real-time reverse transcription PCR panel for detection of severe acute respiratory syndrome coronavirus 2. Emerg Infect Dis 2020;26:1654–65. https://doi: 10.3201/eid2608.201246.
[16] Schwartz DA, Graham AL. Potential maternal and infant outcomes from (Wuhan) Coronavirus 2019-nCoV infecting pregnant women: lessons from SARS, MERS, and other human coronavirus infections. Viruses 2020;12:194. https://doi:10.3390/v12020194.
[17] Labarrere C, Mullen E. Fibrinoid and trophoblastic necrosis with massive chronic intervillositis: an extreme variant of villitis of unknown etiology. Am J Reprod Immunol Microbiol 1987;15:85–91. https://doi:10.1111/j.1600-0897.1987.tb00162.x.
[18] Jacques SM, Qureshi F. Chronic intervillositis of the placenta. Arch Pathol Lab Med 1993;117:1032–5. PMID: 8215826.
[19] Doss BJ, Greene MF, Hill J, Heffner LJ, Bieber FR, Genest DR. Massive chronic intervillositis associated with recurrent abortions. Hum Pathol 1995;26:1245–51. https://doi:10.1016/0046-8177(95)90201-5.
[20] Chen A, Roberts DJ. Placental pathologic lesions with a significant recurrence risk - what not to miss! APMIS 2018;126:589–601. https://doi:10.3109/15513815.2012.659405.
[21] Ordi J, Ismail MR, Ventura PJ, et al. Massive chronic intervillositis of the placenta associated with malaria infection. Am J Surg Pathol 1998;22:1006–11. https://doi:10.1097/00000478-199808000-00011.
[22] Taweevisit M, Sukpan K, Siriaunkgul S, Thorner PS. Chronic histiocytic intervillositis with cytomegalovirus placentitis in a case of hydrops fetalis. Fetal Pediatr Pathol 2012;3:394–400 [https://].
[23] Schwartz DA. Viral infection, proliferation, and hyperplasia of Hofbauer cells and absence of inflammation characterize the placental pathology of fetuses with congenital Zika virus infection. Arch Gynecol Obstet 2017;295:1361–8. https://doi: 10.1007/s00404-017-4361-5.
[24] Lazar M, Perelygina L, Martines R, et al. Immunolocalization and distribution of rubella antigen in fatal congenital rubella syndrome. EBioMedicine 2015;3:86–92. https://doi: 10.1016/j.ebiom.2015.11.050.
[25] Gu J, Xie Z, Gao Z, et al. H5N1 infection of the respiratory tract and beyond: a molecular pathology study. Lancet 2007;370:1137–45. https://doi: 10.1016/S0140-6736(07)61515-3.
[26] Schwartz DA, Caldwell E. Herpes simplex virus infection of the placenta. The role of molecular pathology in the diagnosis of viral infection of placental-associated tissues. Arch Pathol Lab Med 1991; 115:1141–4. PMID: 1747033.
[27] Genen L, Nuovo GJ, Krilov L, Davis JM. Correlation of in situ detection of infectious agents in the placenta with neonatal outcome. J Pediatr 2004;144:316–20. https://doi: 10.1016/j.jpeds.2003.12.015.
[28] Muehlenbachs A, de la Rosa Vázquez O, Bausch DG, et al. Ebola virus disease in pregnancy: clinical, histopathologic, and immunohistochemical findings. J Infect Dis 2017;215:64–9. https://doi: 10.1093/infdis/jiw206.
[29] Gencay M, Puolakkainen M, Wahlström T, et al. Chlamydia trachomatis detected in human placenta. J Clin Pathol 1997;50:852–5. https://doi: 10.1136/jcp.50.10.852.
[30] Li M, Chen L, Zhang J, Xiong C, Li X. The SARS-CoV-2 receptor ACE2 expression of maternal-fetal interface and fetal organs by single-cell transcriptome study. PloS One 2020;15:e0230295. https://doi: 10.1371/journal.pone.0230295.
[31] Pique-Regi R, Romero R, Tarca AL, et al. Does the human placenta express the canonical cell entry mediators for SARS-CoV-2? Elife 2020;9:e58716. https://doi: 10.7554/eLife.58716.
[32] Schwartz DA, Morotti D, Beigi B, Moshfegh F, Zafaranloo N, Patanè L. Confirming vertical fetal infection with COVID-19: neonatal and pathology criteria for early onset and transplacental transmission of SARS-CoV-2 from infected pregnant mothers. Arch Pathol Lab Med 2020 Jul 23. https://doi: 10.5858/arpa.2020-0442-SA.
[33] Schaefer IM, Padera RF, Solomon IH, et al. In situ detection of SARS-CoV-2 in lungs and airways of patients with COVID-19. Mod Pathol 2020;19:1–11. https://doi: 10.1038/s41379-020-0595-z.
[34] Qian GQ, Chen XQ, Lv DF, et al. Duration of SARS-CoV-2 viral shedding during COVID-19 infection. Inf Disp 2020;52:511–2. https://doi: 10.1080/23744235.2020.1748705.
[35] Delorme-Axford E, Sadovsky Y, Coyne CB. The placenta as a barrier to viral infections. Annu Rev Virol 2014;1:133–46. https://doi: 10.1146/annurev-virology-031413-085524.